LASER-INDUCED FLUORESCENCE MICROSCOPY OF COAL MACERALS AND DISPERSED ORGANIC MATERIAL

W.L. Borst, M.W. Pleil,
and G.W. Sullivan
Department of Physics
Texas Tech University
Lubbock, Texas 79409

and

J.C. Crelling and C.R. Landis
Department of Geology
Southern Illinois University
Carbondale, Illinois 62901

INTRODUCTION

Fluorescence microscopy has been a useful analytical tool for characterizing organic material in various coals and rocks (1-9). Teichmuller and Wolf (3,7) discovered new fluorescing coal macerals, which also were found by Spackman (6) in U.S. coals. Ottenjahn et al. (9) related the fluorescence properties of macerals to technological properties of coal. Van Gijzel (8) has organized spectral fluorescence properties for comparison. Since 1983, we have extended fluorescence microphotometry from the spectral to the time domain by using a pulsed laser for fluorescence excitation. Fluorescence decay times are measured as the new characterizing parameters for the dispersed organic material. Simultaneously, individual spectra of the various fluorescing components in the material are obtained. This paper describes the new time-resolved fluorescence microscopy and its application to coal and shale characterization.

SYSTEM DESCRIPTION

The laser fluorescence microscopy system is represented schematically in Figure 1. Further specifications are given in Table 1. A pulsed laser and three sources of continuous wave (c.w.) illumination are interfaced with a Leitz MPV3 microscope. The tungsten lamp is used for spectral calibration and surveying the sample under white light. The mercury and xenon arc lamps are used for fluorescence excitation and are coupled to the excitation monochromator. The EG&G nitrogen pumped dye laser with a BDBP dye provides intense near-ultraviolet light pulses. The laser is coupled to the microscope via a liquid light guide. The modular construction of the microscope allows various optical components to be readily interchanged. The emitted fluorescence is detected by a fast two-stage multichannel plate (MCP) photomultiplier tube (Hamamatsu R1564U-01) with an enhanced red response. The output of the MCP is directed either to a picoammeter when acquiring conventional c.w. spectra or a Tektronics 7912AD fast waveform digitizer when acquiring time-resolved spectra. The digitizer sums a number of MCP output pulses and passes the average to the 4052A Tektronics desk top computer. The extensive software, developed in-house, constitutes a large portion of the development time.

TABLE I - Instrument Parameters and Fluorescence Signals

Size of coal maceral	10-50 μm
Diameter of analyzed area	5 μm
Tuning range of emission monochromator	220-800 nm
Range used	380-800 nm
Monochromator bandwidth	1-7 nm
Continuous Fluorescence Excitation	
Tuning range of excitation monochromator	220-800 nm
Typical excitation wavelength	365 nm
Monochromator bandwidth	1-7 nm
Fluorescence Excitation by Pulsed Laser	
Dye laser pulse duration (FWHM)	0.7 ns
Pulse energy (BDBP dye, 373nm, 10Hz)	10 μJ
Peak power	10 kW
Laser bandwidth (FWHM)	0.04 nm
Dye laser tuning range	360-800 nm
Excitation wavelength used	373 nm
Pulse repetition rate	1-100 Hz
Number of photons emitted per pulse (BDBP dye)	2×10^{13}
Photons onto sample	1×10^{13}
Photons onto measured region of sample ($\sim$5 μm)	$10^{11}-10^{12}$
Typical fluorescence yield	0.001
Photons reaching MCP photomultiplier after passing emission monochromator	10^{4}
Typical number of photoelectrons per pulse	$10^{2}-10^{3}$
Instrument function risetime (laser pulse + photomultiplier + digitizer preamplifier)	0.7 ns
FWHM of instrument function	1.1 ns
Single pulse digitization rate	10-100 GHz
Number of pulses signal averaged, typical	64

METHOD

Time-resolved fluorescence emission spectra are obtained in 10 nm steps by scanning the emission monochromator of the MPV3 from 400 to 700 nm and acquiring the fluorescence decay at each wavelength. This takes about 10 seconds at each wavelength or 5 minutes total. The data reduction yields the multiple decay times, component spectra, and relative intensities and takes about 4 minutes at one wavelength or 1-2 hours total. Conventional spectra are obtained with c.w. illumination and continuously scanning the emission monochromator. This takes about 60 seconds, including correction for optical system response and smoothing. Very similar spectra, as expected, are obtained by integrating the time-resolved results.

For routine data collection, a tungsten lamp is used to determine the spectral response of the system. The lamp is cross calibrated with a standard lamp of a known spectral output. This is done by measuring the raw spectrum, which includes the system response of both the tungsten and standard lamps. The ratio of the raw tungsten spectrum $T_r(\lambda)$ to the raw standard lamp spectrum $E_r(\lambda)$ is independent of the system response, and, when multiplied with the known standard lamp spectrum $E(\lambda)$, results in the true tungsten spectrum $T(\lambda)$

$$T(\lambda) = \frac{T_r(\lambda)}{E_r(\lambda)} E(\lambda) \qquad 1)$$

The determination of the relative spectral response $S(\lambda)$ of a chosen optical configuration (objective, dichroic filter, apertures) is done routinely by measuring the raw tungsten spectrum $T_r(\lambda)$ and dividing by the true tungsten spectrum $T(\lambda)$:

$$S(\lambda) = \frac{T_r(\lambda)}{T(\lambda)} \qquad 2)$$

The corrected fluorescence emission spectrum $R(\lambda)$ from a sample is then determined by taking the ratio

$$R(\lambda) = \frac{R_r(\lambda)}{S(\lambda)} \qquad 3)$$

where $R_r(\lambda)$ is the raw fluorescence spectrum. The above calibration procedures are built into the software. In this way, normalized fluorescence spectra are obtained independently of the particular optical components chosen.

The acquisition and reduction of the pulsed fluorescence data require much care. The individual anode pulses from the MCP PMT contain the fluorescence decay $F(t)$ and the temporal instrument response $I(t)$. The measured signal $M(t)$ is given by the convolution integral

$$M(t) = \int_{-\infty}^{t} I(\tau)\ F(t-\tau)d\tau \qquad 4)$$

The task is to obtain the fluorescence decay function $F(t)$ and, from this, the various decay times and percentage contributions from the individual fluorescing components. This is done with an iterative reconvolution technique and least squares fitting (see below). First, the instrument function has to be determined. If $F(t-\tau)$ in the above integral is a delta-function $\delta(t-\tau)$, then the measured signal $M(t)$ is $I(t)$. Experimentally, a mirror is used in place of the sample, which corresponds to replacing $F(t-\tau)$ with $\delta(t-\tau)$. Thus the instrument response is obtained and contains the contributions from the laser pulse, photomultiplier response and preamplifier bandwidth (1GHz) of the waveform digitizer.

Various deconvolution techniques have been examined by other investigators (15,16,17). We have looked into three such techniques. The software developed allowed us to mathematically model the fluorescence experiments by convoluting a synthesized instrument response, including random Gaussian noise, with an assumed multi-exponential fluorescence decay. The synthesized signal $M(t)$ was then deconvoluted using the different techniques to see how the calculated parameters (decay times and pre-exponential coefficients) compared with the known parameters set at the beginning. We found that the Fourier transform method requires intensive operator interaction and its ability to discern a sum of two or more exponentials was questionable. The method of moments could resolve single and double exponential fluorescence decays. However, extension to three exponential waveforms has proved to be difficult. The technique we found to give the best results is the iterative reconvolution method, which was also found to be most satisfactory by O'Conner et al. (15). We are able to successfully deconvolute data containing up to three different fluorescence decays.

The iterative reconvolution method assumes that the fluorescence decay $F(t)$ from the sample is a sum of exponential terms corresponding to emission from n individual fluorophores:

$$F(t) = \sum_{i=1}^{n} A_i \exp(-t/\tau_i) \qquad 5)$$

Combining this with Equation 4 gives the fitting function

$$M^{o}(t) = \sum_{i=1}^{n} A_i \int_{-\infty}^{t} I(\tau) \exp\left[-(t-\tau)/\tau_i\right] d\tau \qquad 6)$$

where A_i and τ_i are the parameters to be adjusted until a best fit to the measured signal $M(t)$ is found.

This best fit is obtained when the error sum χ^2 is minimized, where

$$\chi^2 = \sum_{i=1}^{N} \frac{1}{\sigma_i^2} \left[M(t_i) - M^{o}(t_i)\right]^2 \qquad 7)$$

and N is the total number of channels (128 or 512) used.

The weight σ_i^2 is the square of the uncertainty in the measurement of the ith channel and is given by

$$\sigma_i^2 = \sigma_0^2 + C\cdot M(t_i) + \left[\frac{\partial M}{\partial t}\right]^2 \sigma_t^2 + \left[\frac{\partial^2 M}{\partial t^2} \frac{\Delta t^2}{2}\right]^2 , \qquad 8)$$

where σ_0^2 is the baseline noise ($0.01 mV^2$), $CM(t_i)$ is the counting error ($1 mV^2$), σ_t is the time axis jitter caused by small fluctuations in the trigger pulse ($\sigma_t \sim 40 ps$) and Δt (~ 0.25 channels) is the fractional channel shift in our time axis lineup routine. Typical values for the last two terms in Equation 8 are $2 mV^2$ and $0.25 mV^2$, respectively.

Minimizing the χ^2 error sum is an iterative process, which involves incrementing the parameters A_i and τ_i and thus successively reducing χ^2. The method employed (20) is a combination of a gradient search along the χ^2 hypersurface and linearization of the fitting function. When far from the surface minimum, the gradient plays the dominant role in determining the increment changes. As the search closes in on the minimum, the linearization of the fitting function dominates. The parameter increments are given by

$$\delta B_j = \sum_{k=1}^{2n} \beta_k \alpha_{jk}^{-1} \qquad 9)$$

where $B_j = (A_i, \tau_i)$, and β_k and α_{jk} are given by the relations:

$$\beta_k = \sum_{i=1}^{N} \frac{1}{\sigma_i^2} \left[M(t_i) - M_e^{o}(t_i)\right] \frac{\partial M_e^{o}(t_i)}{\partial \beta_k} \qquad 10)$$

$$\alpha_{jk} = \sum_{i=1}^{N} \frac{1}{\sigma_i^2} \frac{\partial M_e^{o}(t_i)}{\partial \beta_j} \frac{\partial M_e^{o}(t_i)}{\partial \beta_k} (1+\lambda\delta_{ik}) \qquad 11)$$

$M_e^{o}(t_i)$ is the best fit from the preceding iterations, λ is a weighting factor and δ_{ik} is the Kronecker delta. The weighting factor determines the relative contribution to the increments from the gradient search on the hypersurface to the linearization of the fitting function.

APPLICATION TO COAL MACERAL ANALYSIS

An example for time-resolved fluorescence analysis is given in Figure 2 for a sporinite coal maceral (SIU sample 1444). The top part shows a signal-averaged fluorescence pulse (solid line) and the best 2-exponential fit (dashed line). The emission monochromator was set at 500 nm. The fit yields the pre-exponential coefficients A_i and decay times τ_i. The component percentages are given by

$$P_i = \frac{A_i \tau_i}{\sum_i A_i \tau_i} \qquad \text{(here i=1,2)} \qquad 12)$$

The accuracy of the fit can be assessed from the residuals and the reduced χ_ν^2 (20), where $\chi_\nu^2 \leq 1$ indicates a good fit. Ideally, the residuals should be random. They are not because of a finte number of channels, interpolation between channels, small time axis jitter, and small pulse shape variations. A 2-component decay fits the present data well, and the assumption of a 3-component decay would show redundance in the third component. The quantity τ_m is the mean decay time as defined by $\tau_m = \Sigma P_i \tau_i/100$ and has proved useful for comparisons.

The bottom of Figure 2 shows a complete time-resolved spectral analysis, where the parameters A_i, τ_i, and P_i are plotted versus emitted wavelength. The coefficients $A_i(\lambda)$ are the individual component spectra. The individual decay times τ_i often remain nearly constant over the spectral range, as would be expected for pure substances.

In order to determine the usefulness of time-domain fluorescence analysis as an extension of conventional fluorescence analysis of organic materials, two sets of samples were studied. One set was a series of kerogen-rich shale samples at different levels of maturation from the New Albany Formation from the Illinois Basin. In these samples Type I kerogen is abundant as alginite Tasmanites, and all measurements were taken on this material. While the maturation trends of this material in the Illinois Basin have been studied using vitrinite reflectance and qualitative and quantitative fluorescence techniques (21,22,23), nothing previously was known of the time-resolved fluorescence properties of these (or any) samples. The other set was a series of samples from the lower Kittanning seam from Pennsylvania and Ohio, which range in rank from high-volatile bituminous C to medium-volatile bituminous.

One obvious advantage of the time-resolved analysis is illustrated in Figure 3. The continuous-type fluorescence spectrum for a sample of the alginite Tasmanites (upper diagram) can be time-resolved into two separate spectra (lower diagram). The time-resolved analysis indicates that the continuous spectrum derived from standard fluorescence contains, in this case, the combined contributions from (at least) two fluorescing components with their own distinct spectra.

The fluorescence decay times of organic materials in both sets of samples showed some surprising similarities. First, in all material studied, Tasmanites in the New Albany shale, and fluorinite, sporinite, resinite, and cutinite macerals in the Lower Kittanning seam, the time-resolved data showed good agreement with a two-component decay model. Thus, the fluorescence of all of these materials appears to be composed of two fluorescing components with lifetimes in the subnanosecond and nanosecond ranges. In addition, the fast lifetime component (about 200 ps) seems to be constant in all samples and maceral types. Although these results are preliminary, a working hypothesis is that the two fluorescence lifetimes are from two different fluorophores, one of which is common to all the materials studied (alginite, fluoronite, resinite, cutinite and sporinite).

When the fluorescence decay times were plotted against rank (as defined by vitrinite reflectance), the alginites and sporinites showed the clearest trends as seen in Figures 4 and 5. The decay times do not seem to change much with increase in thermal maturation or rank. However, the percentage contribution of each component to the overall spectra do show a systematic change as illustrated in the same figures. In the case of the alginite, the fast component increases with rank, the slow component decreases, and the trends are reversed for the sporinites. Although these data are preliminary, the hypothesis (being investigated further) is, that in the maturation process one fluorophore is transforming into another.

To further test our experimental procedures, model compounds (e.g. POPOP, anthracene) in solution and their mixtures were studied. We found that two compounds can be distinguished in a mixture and the correct fluorescence decay times and spectra are obtained.

CONCLUSIONS

1. Time-domain analysis is a powerful extension of continuous fluorescence analysis.
2. Characteristic lifetimes, percentages, and intensities can be determined.
3. The spectra of a variety of organic materials can be resolved into two distinct components, one in the subnanosecond range and one in the nanosecond range.
4. Within the resolution limits of the system (100 ps), it appears that the fast lifetime component is the same in a variety of organic materials.
5. With the new technique, mixtures of short and long lifetime model compounds can be resolved into their original component spectra and fluorescence decay times.
6. In alginites and sporinites, fluorescence lifetimes appear to be nearly constant with changes in rank.
7. In alginites and sporinites, the percentage contribution from each component changes with rank.

Time-resolved laser spectroscopy improves the specificity of conventional fluorescence microphotometry of coals and oil shales. We have been using the new technique in studies of dispersed organic matter in shales and expect to understand better the maturation of the organic material in source rocks (24).

ACKNOWLEDGEMENTS

Support from the U.S. Department of Energy (Grant DE-FG22-82PC 50801) and E. Leitz, Inc., is gratefully acknowledged.

REFERENCES

1. P. van Gijzel, "Autofluorescence of Fossil Pollen and Spores with Special Reference to Age Determination and Coalification", Leidse Geol. Meded., Vol. 50, pp. 263-317 (1967).
2. H. Jakob, "Lumineszenz-Mikroskopie der Organo-Petrographischen Bestandteile von Sedimentgesteinen", Leitz-Mitteilungen Wiss. u. Tech., Vol. 4, no. 8, pp. 250-254 (1969).
3. M. Teichmuller, "Uber Neue Macerale der Liptinit-Gruppe und die Entstehung von Micrinit," Fortschr. Geol. Rheinld. und Westf., Vol. 24, p. 37-64 (1974).
4. P. van Gijzel, "Polychromatic UV Fluorescence Microphotometry of Fresh and Fossil Plant Substances with Special Reference to the Location and Identification of Dispersed Organic Material in Rocks", Petrographie Organique et Potentiel Petrolier, ed. by B. Alpern, pp. 67-91, CNRS, Paris (1975).

5. K. Ottenjann, M. Teichmuller, and M. Wolf, "Spectral Fluorescence Measurements in Sporinites in Reflected Light and Their Applicability for Coalification Studies", in Petrographie Organique et Potentiel Petrolier, ed. by B. Alpern, pp. 49-65, CNRS, Paris (1975).
6. W. Spackman, A. Davis, and G.D. Mitchell, "The Fluorescence of Liptinite Macerals", Brigham Young University Geology Studies, Vol. 22, pp. 59-75 (1976).
7. M. Teichmuller and M. Wolf, "Application of Fluorescence Microscopy in Coal Petrology and Oil Exploration", J. of Microscopy, Vol. 109, pp. 49-73 (1977).
8. P. van Gijzel, "Recent Developments in the Application of Quantitative Fluorescence Microscopy in Palynology and Paleobotany", Annales des Mines de Belgique, pp. 165-181, July-August (1978).
9. K. Ottenjann, M. Wolf, and E. Wolf-Fischer, "Beziehungen zwischen der Fluoreszenz von Vitriniten and den Technologischen Eigenschaften von Kohlen", Proc. of the International Conference on Coal Science, Dusseldorf, Germany, IEA, pp. 86-91 (1981).
10. W.L. Borst, H.A. Hamid, J.C. Crelling, "Laser Induced Fluorescence Microscopy", Int. Conf. on Coal Sci., Pittsburgh, Penn; publ. by Int. Energy Agency, pp. 649-652 (1983).
11. W.L. Borst, G.W. Sullivan, H.A. Hamid, "Pulsed Laser Induced Fluorescence Microscopy for Materials Characterization", Bull. of the Amer. Phys. Soc., Vol. 28/29, p. 1335 (1983).
12. G.W. Sullivan and W.L. Borst, "Introduction to Fluorescence Spectroscopy of Coal Macerals", NATO Advanced Study Institute on Application of New Spectroscopic Techniques to Coal Science, St. Francis Xavier University, Antigonish, Canada, August 1984 (in press).
13. W.L. Borst, G.W. Sullivan, and R.N. Zitter, "Laser Induced Fluroescence Spectroscopy", NATO Advanced Study Institute (same as above; in press).
14. G.W. Sullivan, W.L. Borst, M.W. Pleil, and C.L. Landis, "The Application of Pulsed Laser Fluorescence Microscopy to Coal Maceral Characterization", NATO Advanced Study Insititute (same as above; in press).
15. D.V. O'Conner, W.R. Ware, and J.C. Andre, J. Phys. Chem., 83, p. 1333 (1979).
16. A.Grinvald, I.Z. Steinberg, Anal. Biochem., 59, p. 583 (1974).
17. R.B. Cundall, R.E. Dale, "Time-Resolved Fluorescence Spectroscopy in Biochemistry and Biology", Plenum Press, New York (1983).
18. J.R. Lakowicz, "Principles of Fluorescence Spectroscopy," Plenum Press, New York (1983).
19. W. Demtroder, "Laser Spectroscopy - Basic Concepts and Instrumentation", Springer Verlag; Berlin, New York (1981).
20. P.R. Bevington, "Data Reduction and Error Analysis for the Physical Sciences", McGraw-Hill, New York (1969).
21. M.H. Barrows, R.M. Cluff, AAPG Memoir 35: Petroleum Geochemistry and Basin Evaluation, p. 111 (1984).
22. M.H. Barrows, R.M. Cluff, R.D. Harvey, Proc. 3rd Eastern Gas Shale Symp., p. 85 (1979).
23. G.E. Cox, M.S. Thesis, Southern Illinois University at Carbondale (1985).
24. Pieter van Gijzel, "Applications of the Geomicrophotometry of Kerogen, Solid Hydrocarbons, and Crude Oils to Petroleum Exploration", publ. in Organic Maturation Studies and Fossil Fuel Exploration, ed. J. Brooks, Academic Press (London, 351-377 (1981).

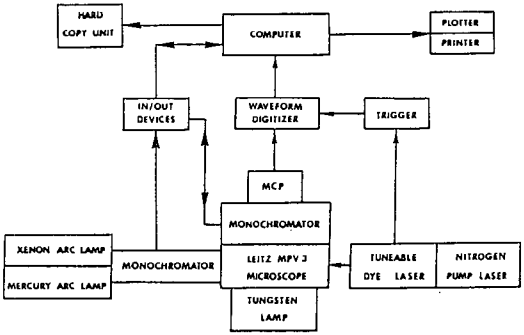

Figure 1. Schematic diagram of the apparatus. Fluorescence pulses from the specimens (coal, shale) in the microscope are excited by pulsed laser, spectrally analyzed, and acquired with the digitizer for subsequent time-domain analysis by computer. For continuous wave excitation, a picoammeter (not shown) is connected to the MCP photomultiplier and computer.

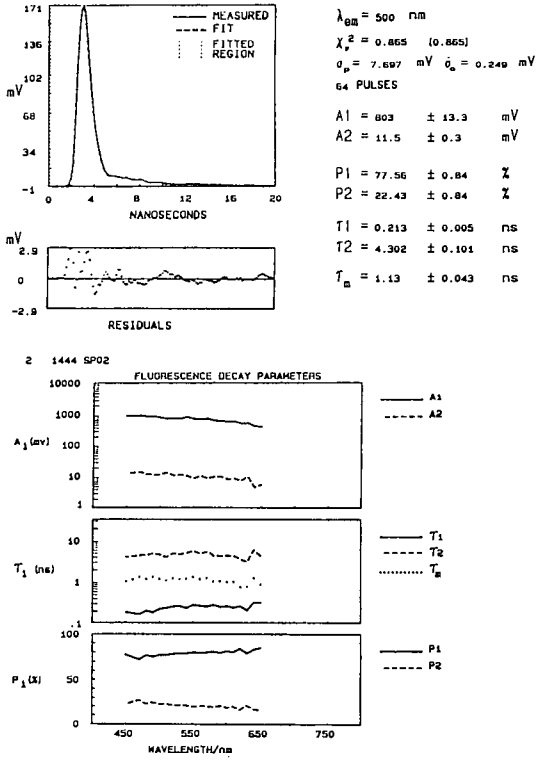

Figure 2. Example of time-resolved fluorescence from a sporinite coal maceral (lower Kittaning seam). The top part shows the results for the fluorescence pulses emitted at a single wavelength. The bottom part shows the wavelength dependence of the pre-exponential coefficients $A_i(\lambda)$ (i.e. time-resolved spectra), fluorescence decay times τ_i, and percentage contributions P_i from the fluorescing compounds.

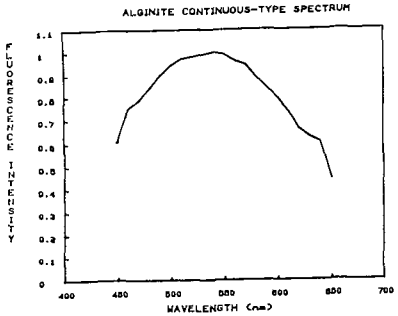

Figure 3a. Composite fluorescence spectrum from an alginite maceral in New Albany shale. The spectrum was obtained by integrating the fluorescence pulses over time and is similar to that measured with continuous wave excitation.

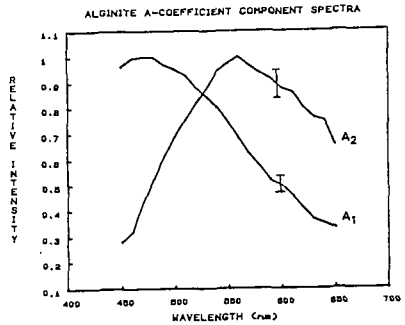

Figure 3b. Resolution of the composite spectrum above into two time-resolved component spectra (normalized to the same height). The vertical uncertainty bars indicate the 2σ - range of the two individual spectra for 45 alginite macerals of different rank.

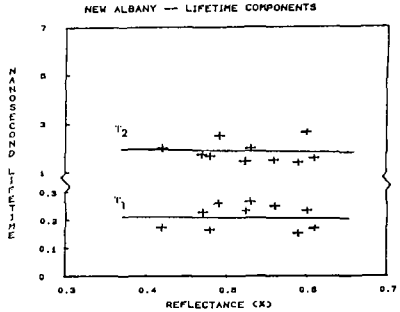

Figure 4a. The two fluorescence decay times in alginite Tasmanites from the New Albany formation (Illinois Basin) as a function of vitrinite reflectance (rank). Each data point is an average over 3 to 5 macerals and over the fluorescence emission spectrum.

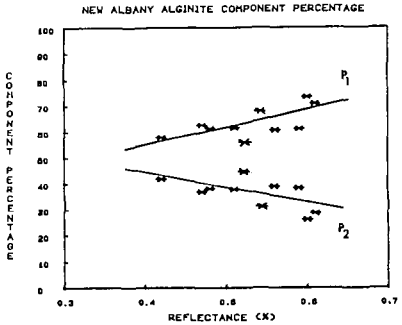

Figure 4b. The percentage contributions to the fluorescence from the two time-resolved components in alginite as a function of vitrinite reflectance. The averaging is the same as in Figure 4a.

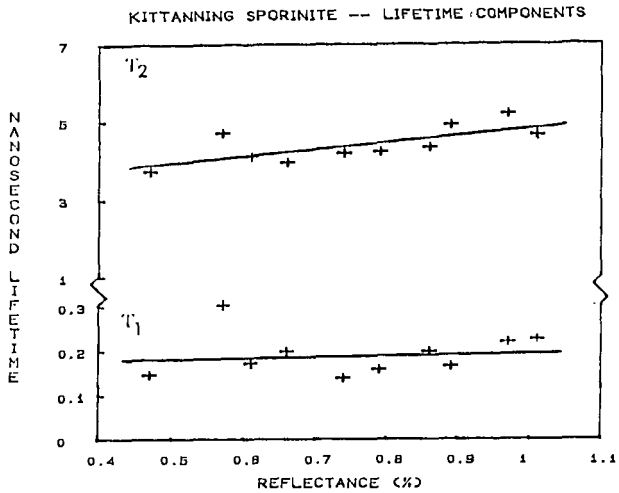

Figure 5a. The resolved fluorescence decay times from sporinite coal macerals from the lower Kittaning seam (Pennsylvania and Ohio) as a function of rank. (See also caption to Figure 4a.)

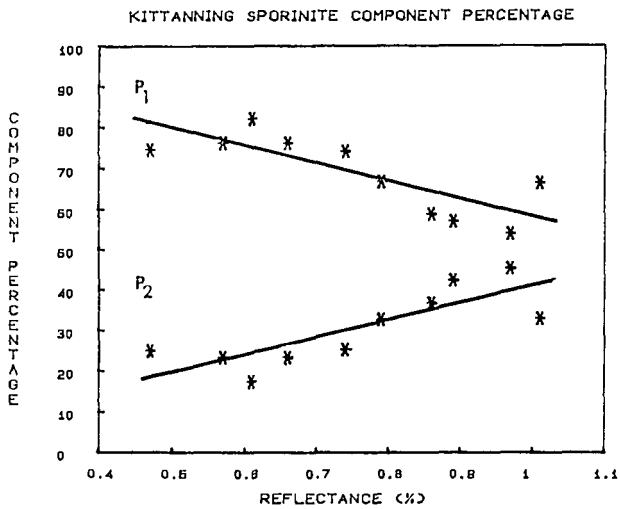

Figure 5b. Percentage contributions to the fluorescence from the two major fluorescing components in sporinite as a function of vitrinite reflectance. (See also caption to Figure 4b.)